# Supplementary

## S1. Refractive index of crystalline silicon

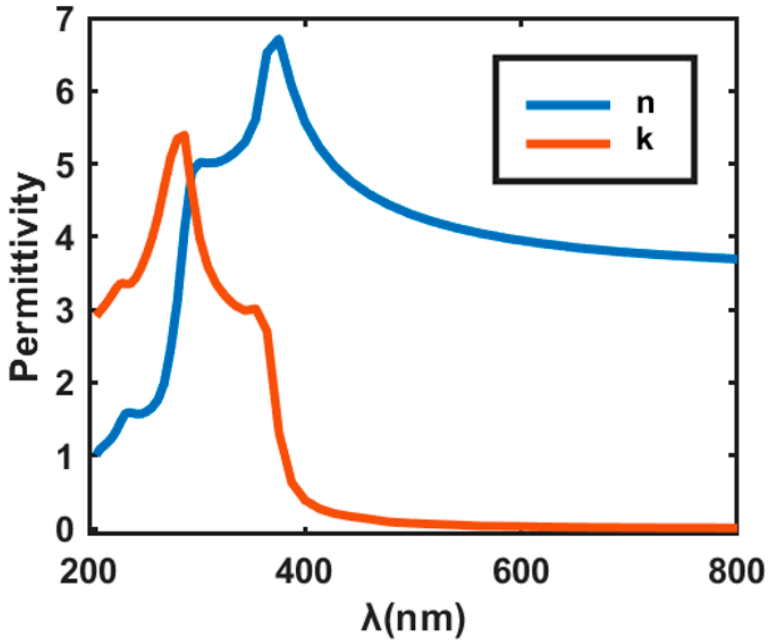


**Figure S1**. The complex refractive index of crystal silicon. The complex refractive index $\tilde{n}=n+ik$, the real part $n$ shows in blue line, and the imaginary part $k$ shows in orange line.

## S2. Focusing performance at other wavelengths

To investigate the focusing performance of the metalens at wavelengths outside the design range, we simulated the performance for oblique incident light at 488 nm, 510 nm, 532 nm, 550 nm, 610 nm, and 633 nm using FDTD. The metalens has an NA of 0.7 and a theoretical focal length of f =21 μm. Figure S2 shows the light intensity distribution of the outgoing light field in the xz plane for each wavelength. The focal spots for the designed wavelengths of 488 nm, 532 nm, and 633 nm are in good agreement with the theoretical values. However, the focal spots for several non-designed wavelengths deviate from the theoretical values. The focusing efficiency of the metalens at the theoretical focal length for wavelengths of 510 nm, 550 nm, and 610 nm is 0.009%, 0.031%, and 0.016%, respectively, indicating an unsatisfactory focusing performance.

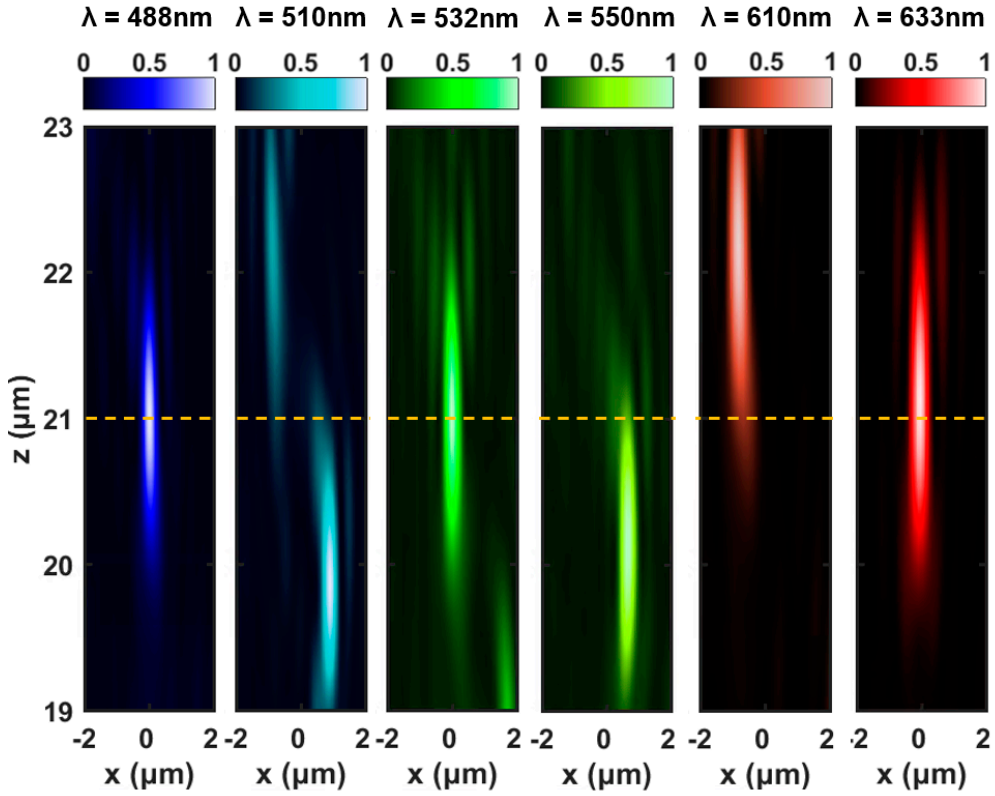


**Figure S2** Simulated light intensity profiles for the RGB achromatic metalens (NA=0.7) at various incident wavelengths. The yellow dashed line indicates the position of the focal plane. The designed RGB wavelengths are 488 nm, 532 nm and 633 nm, respectively.

## S3. Analysis on large-angle deflection for large FOV

In our design, both the own phase response and the coupling between adjacent nanostructures are taken into consideration. Based on our analysis, the FDTD simulation confirms that the metalens designed in this method is effective. The actual phase distribution of light being reflectively focused by the metalens (depicted in Figure S3) shows that the output light wavefront gradually converges to the focal spot, even for the light that requires a large deflection angle at the edge area of the metalens. This indicates that the metalens can realize effective NA consistent with the design value.

Moreover, the measured FWHMs of the three-wavelength focusing spots (Figure 3 in the main text) are close to the FWHMs at the diffraction limit for NA = 0.7 according to $\lambda/2NA$, indicating that the metalens can provide focusing performance consistent with the designed numerical aperture. The measured FWHMs are 456 nm, 405 nm, and 375 nm for R, G, and B, respectively. Therefore, the metalens can efficiently modulate and collect the reflected light from large angles, allowing the large FOV designed in this paper to be realized.

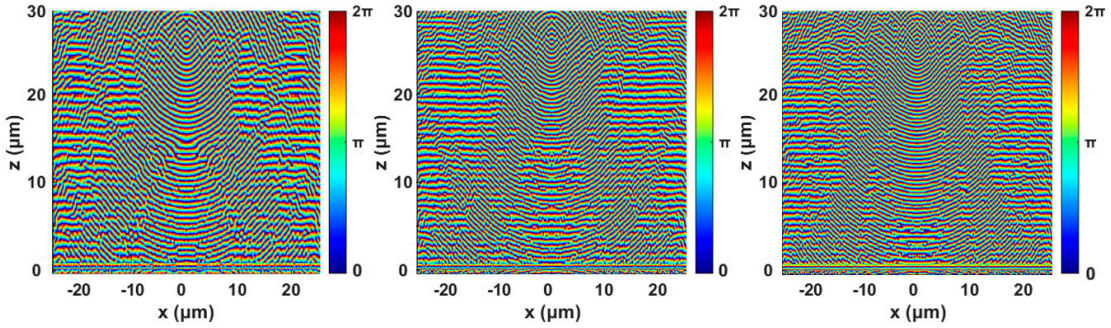


**Figure S3.** The phase distribution of the outgoing light field pass through the metalens with diameter = 50 μm and NA=0.7. (a) 633nm. (b) 532nm. (c) 488nm.

## S4. Transmission for obliquely incident ambient light

To account for the fact that ambient light can come from various directions, the phase distribution of broadband obliquely incident ambient light passing through the metalens is also simulated. For example, taking oblique incident ambient light with an angle of $\theta$=10°, as shown in Figure S4, the metalens is observed to not noticeably affect the wavefronts of the obliquely incident ambient light. As a result, the transmitted light traveled into free space along the original incidence direction without any significant phase distortion.

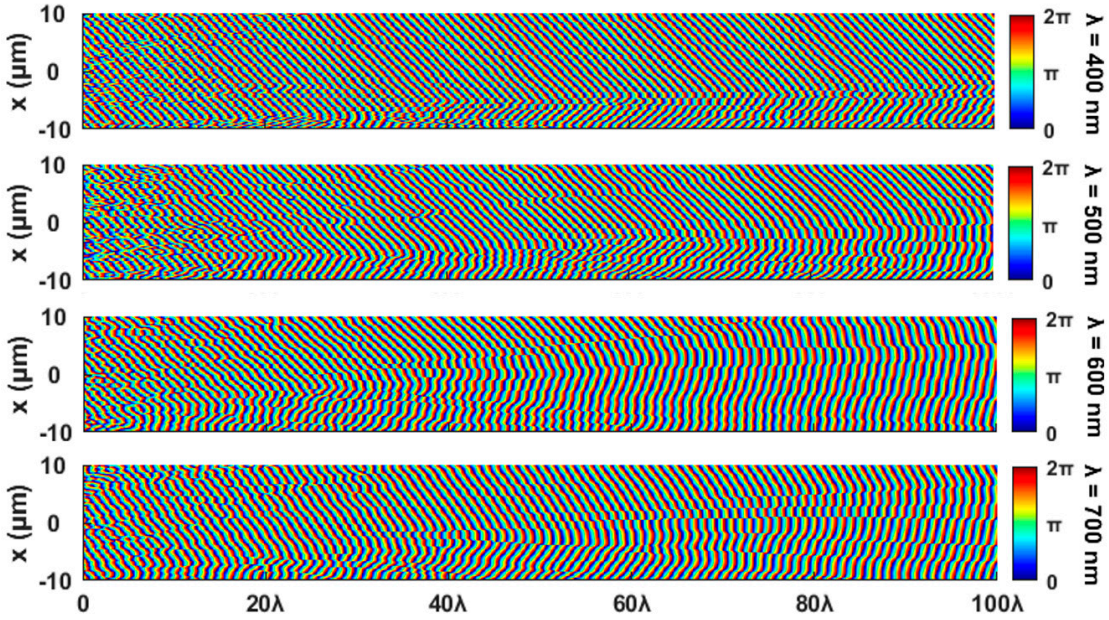


**Figure S4.** The phase distributions of obliquely incident light ($\theta$=10°) at various wavelengths passing through the metalens. It demonstrates that the metalens does not significantly affect the wavefronts of the obliquely incident light, and the transmitted light travels into free space along the original incidence direction without any noticeable phase distortion.

## S5. Other material combinations

Silicon nitride is a material with high transmission to visible light that it is one of the candidates for metalenses. Here, we try to compare the silicon nitride platform with the crystalline silicon platform for the proposed AR metalens.

For a meta-unit, the silicon nitride nanopillar seats on the silica substrate as shown in Figure S5(a), and other schemes combining with different thin layers are also investigated. As the focusing of the AR metalens is in the reflection mode, the reflectance is of the priority to be evaluated. Taking the cylindrical nanopillars as examples, the reflectance and transmission maps for different geometrical combinations are scanned by FDTD software as shown in Figure S5(b) and (c), respectively.

Table S1 summarizes the reflective focusing efficiencies for different schemes. It can be seen that the reflectance is too low to perform reflective focusing for the scheme with only silicon nitride nanopillars (scheme I); hence, this scheme is not considered to be used in the AR metalens. Then, the focusing performance based on other schemes are simulated by the same designing method. Table S1 shows the simulated focusing results of the corresponding metalenses for oblique p-polarized incident light with the same diameter of 1 mm and NA = 0.7. The reflective focusing efficiencies do not have overwhelming advantages compared with the results in main text, showing that the c-Si material scheme is effective. The normalized intensity distributions of these focal spots are shown in Figure S6. Stray light is obviously seen near the focal spots, which may be attributed to the low efficiencies of these configurations.

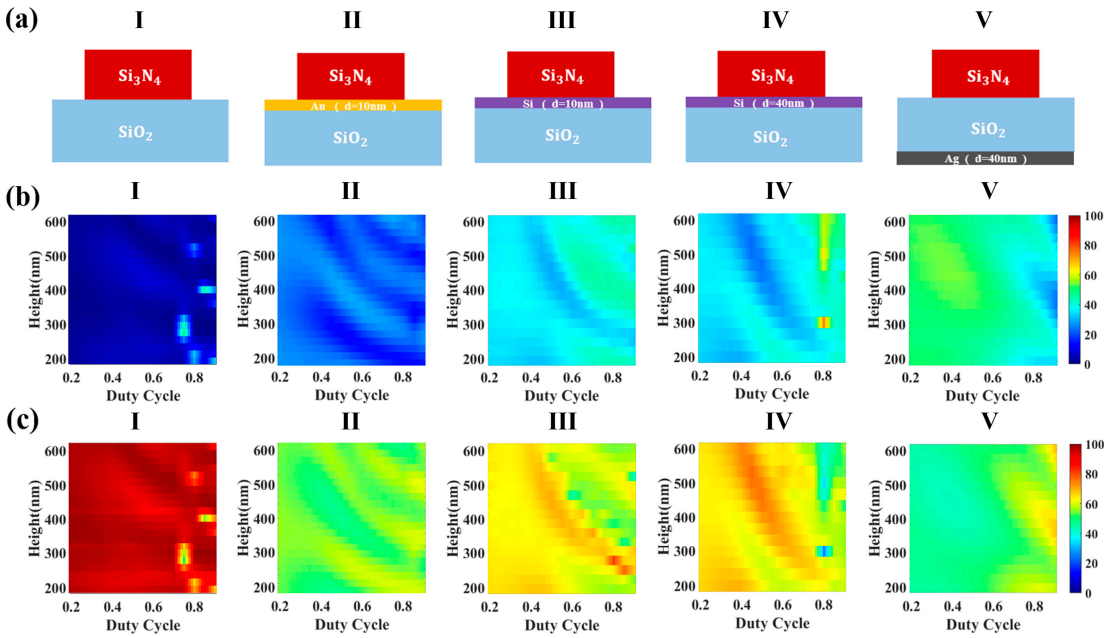


**Figure S5**. **(a)** Schemes of different meta-units with cylindrical nanopillars made of silicon nitride. **I.** $Si_3N_4$: $SiO_2$; *II.* $Si_3N_4$:Au(10 nm):$SiO_2$; *III.* $Si_3N_4$:Si(10 nm):$SiO_2$; *IV.* $Si_3N_4$:Si(40 nm):$SiO_2$. *V.* $Si_3N_4$:$SiO_2$:Ag(40 nm). **(b)** The corresponding reflectance maps and **(c)** transmission maps. Duty cycle = diameter/period.

**Table S1.** Reflective focusing efficiencies for different schemes

| | H (nm) – U (nm) | Reflective focusing efficiency | | |
|---|---|---|---|---|
| | | R | G | B |
| I | - | - | - | - |
| *II* | 440 - 380 | 8.59% | 1.86% | 0.12% |
| *III* | 360 - 320 | 8.96% | 3.87% | 1.06% |
| *IV* | 400 - 320 | 9.02% | 4.57% | 4.55% |
| *V* | 580 - 380 | 8.77% | 4.61% | 2.15% |
| *c-Si* | 175 - 200 | 8.73% | 10.55% | 4.18% |

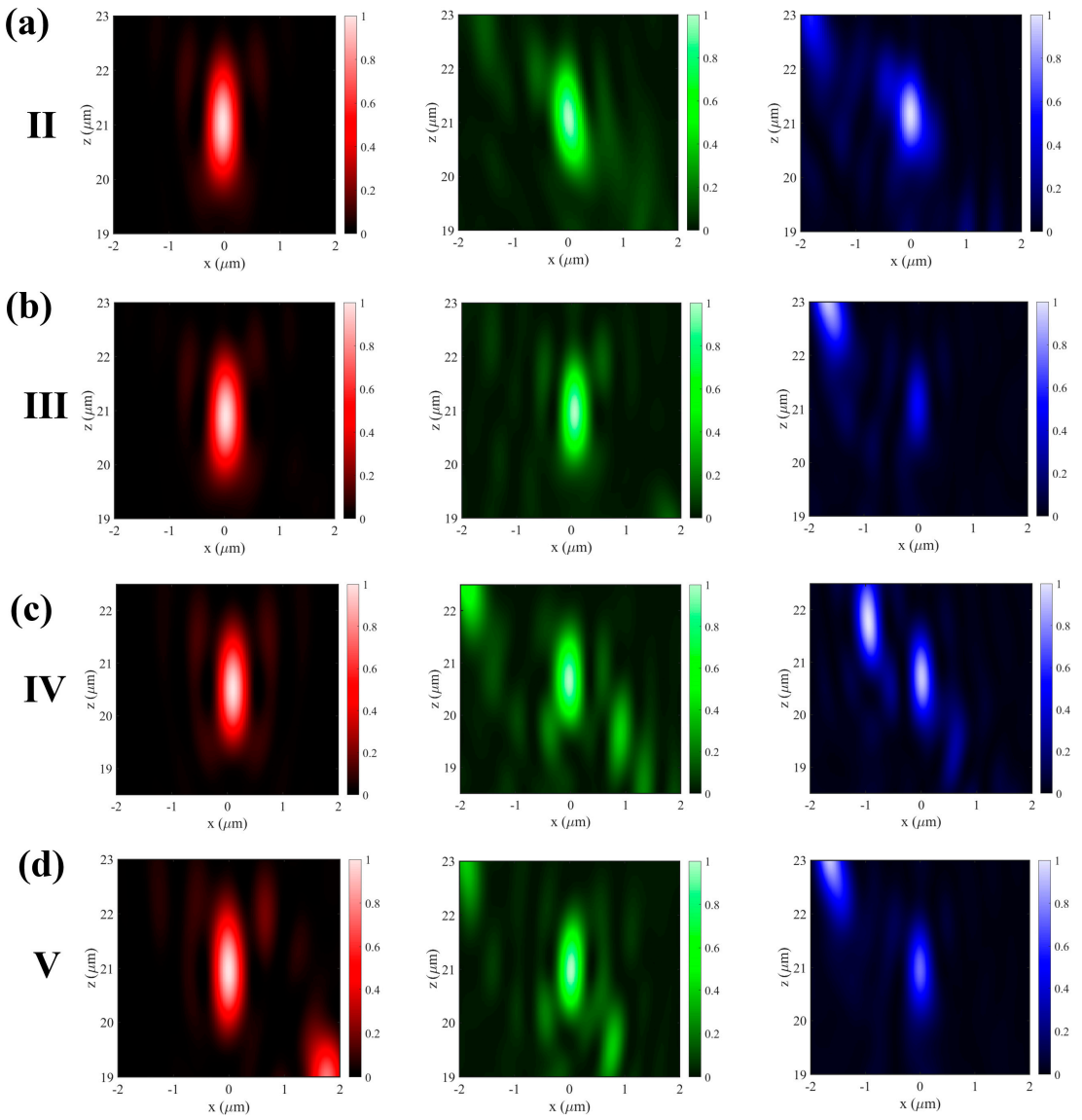


**Figure S6.** Simulated normalized intensity distributions of metalenses with the material platforms corresponding to scheme II to V. Red, green, and blue colors correspond to the wavelengths of 633 nm, 532 nm, and 488 nm, respectively.